Chemical Engineering Science 174 (2017) 25–39

Contents lists available at ScienceDirect

Chemical Engineering Science

journal homepage: www.elsevier.com/locate/ces

Simulation of bubbly flows with special numerical treatments of the semi-conservative and fully conservative two-fluid model

Dongyue Li [a,b,*], Hasse Christian [b]

[a] Institute of Fluid Dynamics, Helmholtz-Zentrum Dresden-Rossendorf, 01314 Dresden, Germany
[b] Numerical Thermo-Fluid Dynamics, Department of Energy Process Engineering and Chemical Engineering, TU Bergakademie Freiberg, Fuchsmuehlenweg 9, 09599 Freiberg, Germany

HIGHLIGHTS

- The semi-conservative and fully conservative implementation in the two-fluid model are validated.
- Different test cases for turbulent gas-liquid dispersions in a bubble column are simulated.
- The drag force is calculated by the linear blending method and the hyperbolic blending method.
- The blending method is more versatile than the traditional method and offers significant advantages applications.

GRAPHICAL ABSTRACT

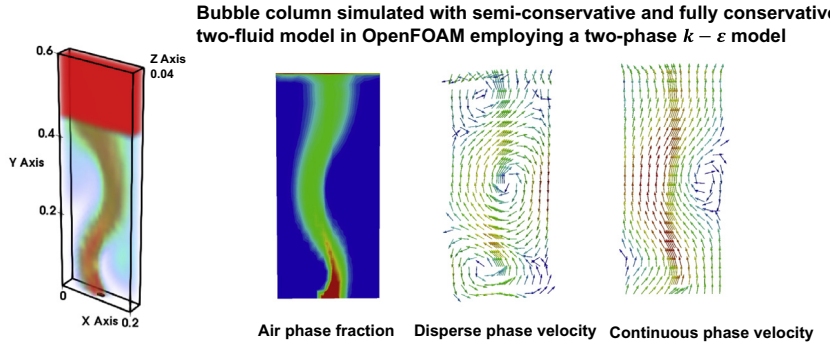

ARTICLE INFO

Article history:
Received 16 May 2017
Received in revised form 27 July 2017
Accepted 30 August 2017
Available online 1 September 2017

Keywords:
Bubble column
Two-fluid model
CFD
Frag force
OpenFOAM

ABSTRACT

Bubbly flows are found in a large number of chemical engineering applications. For the computational fluid dynamics (CFD) simulations of such multi-phase flows, both physical models and numerical treatment are crucial to obtain robust and accurate results. In this numerical study, we investigate the two-fluid model (TFM) under challenging conditions such as phase segregation and inversion. For the phase segregation, a singular problem arises in the phase momentum and the two-phase $k-\varepsilon$ equations when one phase fraction approaches zero. Another numerical issue is the accurate calculation of the drag coefficient, e.g., during the phase inversion. To address the singular problem, previous studies used a non-conservative formulation after dividing by the phase fraction; in our approach, we present a robust methodology for semi-conservative and fully conservative formulations. A special numerical treatment is introduced to the phase momentum equations and the turbulence equations, which avoids the singular problem in case of phase segregation. Concerning the drag force, two novel methods, the linear and the hyperbolic blending method, respectively, are presented to obtain accurate results. For testing the new numerical treatment, the analytical solution of a two-dimensional test case is first compared with the results predicted using a semi-conservative and a fully conservative formulation. The second test case investigated is a bubble column with different superficial velocities. The results from three-dimensional simulations using the novel formulations show good agreement with the literature data. Especially when phase segregation occurs, the semi-conservative and the fully conservative formulations using the two-phase $k-\varepsilon$ model formulation converge.

* Corresponding author at: Institute of Fluid Dynamics, Helmholtz-Zentrum Dresden-Rossendorf, 01314 Dresden, Germany.
E-mail address: dongyue.li@hzdr.de (D. Li).

http://dx.doi.org/10.1016/j.ces.2017.08.030
0009-2509/

1. Introduction

Two-phase bubble columns are widely used in the chemical and biochemical industries for carrying out gas-liquid and gas-liquid-solid reaction processes, as shown by Deckwer and Field (1992), Becker et al. (1999), Behzadi et al. (2004, 2005), Shaikh and Al-Dahhan (2007), Lau et al. (2013), Jain et al. (2014), Singh et al. (2017). Flows in this type of equipment can be described using partial differential equations (PDEs), which cannot be solved analytically except in very special cases. For process design and analysis, computational fluid dynamics (CFD) has become an important and indispensable tool. Specifically, the simulation methods for bubbly flows in CFD can be divided into the following models: the discrete element model (DEM) (Cundall and Strack, 1979; Brilliantov et al., 1996; Wang et al., 2017), the discrete particle model (DPM) (Hoomans et al., 1996; Zhu et al., 2007; Buwa et al., 2006; Besbes et al., 2015), and the two-fluid model (TFM) (Ishii, 1975; Drew, 1982; Ishii and Mishima, 1984; Drew and Passman, 2006; Ishii and Hibiki, 2010; Lopez De Bertodano et al., 2016). In this research, we focus on using TFM to predict gas-liquid dispersions in a bubble column. It uses the Eulerian approach, in which both phases are treated as interpenetrating continua and suitably averaged momentum equations are solved for both (Oliveira and Issa, 2003). Thus, the model is expressed in terms of two sets of conservation equations governing the balance of mass, momentum, and energy for each phase. However, the fields of each phase interact with the other phase, which is explained by an interaction term appearing in the balance equations. TFM is anticipated to predict more accurate details than the mixture model (Ishii, 1977; Hibiki and Ishii, 2003), as the variables are governed by their own balance equation. Comprehensive details about the governing equations of TFM can be found in Ishii and Hibiki (2010) and Lopez De Bertodano et al. (2016), which were published recently.

Even though the governing equations of TFM are well defined, it is usually not possible to obtain the solution if the equations are solved without any special numerical treatment. The TFM was found to be ill-posed in regions of higher dispersed phase fractions (dispersed phase fraction $> 26\%$) and a grid restriction is usually employed on TFM to avoid an ill-posed problem (Vaidheeswaran and Lopez De Bertodano, 2017). Apart from that, it was shown by Oliveira and Issa (2003) that the iterative TFM algorithms invariably led to numerical problems, especially when there is segregation of the phases or when recirculation zones occur. When the phase fraction tends to zero, the phase momentum equation also becomes singular. This singular problem was handled by Oliveira and Issa (2003) and Weller (2002) by dividing the phase momentum equations by the phase fraction. This numerical treatment is used in many CFD codes such as TRACE (Bajorek, 2008), MARS (Jeong et al., 1999), ACE 3D (Yoshida et al., 2008), OpenFOAM-1.7.x (`bubbleFoam`), and some in-house codes (Saurel and Abgrall, 1999). Oliveira and Issa (2003) adopted the non-conservative phase momentum equations to calculate the two-phase sudden expansion flows. The decay in the phase velocity residuals calculated from the non-conservative phase momentum equations on two meshes showed no convergence problems. Rusche (2003) also employed the non-conservative phase momentum equations to simulate a two-phase sudden enlargement pipe and a bubble plume, and good agreement was obtained with the experimental data. Recently, Liu and Hinrichsen (2014) also coupled the non-conservative phase momentum equations with the population balance model (PBM) to simulate bubble columns.

The main disadvantages of this approach are that the phase momentum equations are transformed into non-conservative ones and compressibility effects are neglected. Park et al. (2009) proposed using another form of the phase momentum equations. In this approach, the phase momentum equations are conservative in space and non-conservative in time. In the case of a steady state, they reduce to the conservative form. The algorithm of Park et al. (2009) was implemented in CUPID. In OpenFOAM-2.1.1, other semi-conservative phase momentum equations were also developed and implemented as `compressibleTwoPhaseEulerFoam`, together with a single-phase $k-\varepsilon$ model. In this solver, the volume of each phase is conservative. One of the key differences between the non-conservative formulations and the semi-conservative formulations is that there is a source term in the pressure Poisson equation to explain the compressibility effects. Another difference is that a special numerical treatment of the drag force is developed to prevent singular problems. Buffo et al. (2013a) employed the semi-conservative phase momentum equations coupled with the population balance model (PBM) to simulate bubble columns. Their predicted plume oscillation period and gas hold-up agreed well with the experimental data. Passalacqua and Fox (2011) also employed the semi-conservative phase momentum equations to simulate multi-fluid gas-particle flows on unstructured grids; a comparison of their results with MFIX showed that semi-conservative phase momentum equations can properly predict the behavior of the systems under their investigation. Li et al. (2017), Li et al. (in press) employed the same approach to simulate the liquid-liquid dispersions in stirred tanks.

The TFM with the single-phase $k-\varepsilon$ model has been employed in many works (Petitti et al., 2010; Maaß et al., 2010; Li et al., 2017; Buffo et al., 2016; De Bona et al., 2016; Buffo et al., 2016) for various reasons. One reason is that it saves computational resources. Another is that the singular problem does not occur for a single-phase $k-\varepsilon$ model, which is also a main reason preventing the two-phase $k-\varepsilon$ model from becoming popular. Only a few works have employed the two-phase $k-\varepsilon$ model to simulate two-phase flows (Behzadi et al., 2004; Bhusare et al., 2017), and the numerical treatments preventing the singular problem in the turbulent equations are not clear. In the recently distributed OpenFOAM-4.0, the `twoPhaseEulerFoam` multiphase solver has been rewritten to be fully conservative in terms of mass, momentum, and energy. The single-phase $k-\varepsilon$ model was also extended to be a two-phase turbulence model. Special numerical treatments of the source term were also adopted to prevent the singular problems. In contrast to the approach of dividing by the phase fraction in the governing equations resulting in a non-conservative formulation, the essence of the semi-conservative and fully conservative formulations is to degenerate the differential equations into algebraic equations in those cells where the phase fraction is null. Moreover, to prohibit non-physical predictions of the drag force, the developers of OpenFOAM-4.0 implemented two different methods in it following the initiative idea from Weller (2002) and Rusche (2003), namely, the linear blending method and the hyperbolic blending method.

In this study, we investigated a numerical approach to prevent singular problems by specially treating the drag force for semi-conservative and fully conservative phase momentum equations and by adding a numerical source term for two-phase turbulent equations. At first, the derivations for the semi-conservative and fully conservative phase momentum equations, together with the construction of the pressure Poisson equations and the phase fraction equation, are presented to show how to ensure the boundedness and robustness of the discretization algorithm implemented. The two-phase $k-\varepsilon$ model with a special source term is also presented. Then, the numerical treatment of the drag force using the traditional method, linear blending method, and hyperbolic method is discussed. The semi-conservative and fully conservative formulations are compared with an analytical solution for a simple test case. A bubble column test case (3D) from Díaz et al. (2008) is

considered to investigate the effect of the different numerical treatments of the drag force and the effect of the different semi-conservative and fully conservative phase momentum equations on the results. The predicted flow fields are also compared with the literature data. To our knowledge, the numerical approach of preventing singular problems by adding a source term in the momentum equations and two-phase turbulence equations, together with the special numerical treatment of the drag force using the blending methods, has never been discussed and validated in the literature.

2. Governing equations and implementations

The TFM equations are based on conditioning technology (Hill, 1998). They are applied to two-phase flows by considering the phases as being separated by an infinitesimally thin interface. An indicator function I_ϕ is defined previously, which is 1 in phase ϕ and 0 in the other phases. The continuity equation, momentum equation, and energy equation in the TFM are conditionally averaged by multiplying I_ϕ and then applying a conventional averaging technique, density weighted or otherwise. More details about the conditional averaging were described by Dopazo (1977). The current work focuses on the numerical treatment of the TFM in CFD simulations for bubbly flows. Hence, the heat transfer and mass transfer are neglected here. Under such assumption, the conservation of mass for phase a and phase b can be expressed by Drew (1982):

$$\frac{\partial(\alpha_a\rho_a)}{\partial t}+\nabla\cdot(\alpha_a\rho_a\mathbf{U}_a)=0, \tag{1}$$

$$\frac{\partial(\alpha_b\rho_b)}{\partial t}+\nabla\cdot(\alpha_b\rho_b\mathbf{U}_b)=0, \tag{2}$$

where α_a and α_b are the phase fraction of phase a and phase b, ρ_a and ρ_b are the density for phase a and phase b, and $\mathbf{U}_a$ and $\mathbf{U}_b$ are the average velocity for phase a and phase b, respectively.

The average velocities $\mathbf{U}_a$ and $\mathbf{U}_b$ can be calculated by solving the corresponding phase momentum equations (Drew, 1982):

$$\frac{\partial(\alpha_a\rho_a\mathbf{U}_a)}{\partial t}+\nabla\cdot(\alpha_a\rho_a(\mathbf{U}_a\otimes\mathbf{U}_a))+\nabla\cdot(\alpha_a\rho_a\boldsymbol{\tau}_a)+\nabla\cdot(\alpha_a\rho_a\mathbf{R}_a)=-\alpha_a\nabla p_a+\alpha_a\rho_a\mathbf{g}-\mathbf{M}, \tag{3}$$

$$\frac{\partial(\alpha_b\rho_b\mathbf{U}_b)}{\partial t}+\nabla\cdot(\alpha_b\rho_b(\mathbf{U}_b\otimes\mathbf{U}_b))+\nabla\cdot(\alpha_b\rho_b\boldsymbol{\tau}_b)+\nabla\cdot(\alpha_b\rho_b\mathbf{R}_b)=-\alpha_b\nabla p_b+\alpha_b\rho_b\mathbf{g}+\mathbf{M}, \tag{4}$$

where p_a and p_b are the pressure for each phase, $\boldsymbol{\tau}_a$ and $\boldsymbol{\tau}_b$ are the laminar viscous-stress tensors, $\mathbf{R}_a$ and $\mathbf{R}_b$ are the Reynolds stress tensors, $\mathbf{g}$ is the gravitational acceleration vector, and $\mathbf{M}$ is the interfacial force exchange term.

Because the phase equations and momentum equations for each phase are of a similar type, in the following, we use φ to represent the variable for a certain phase. For a Newtonian fluid, $\boldsymbol{\tau}_\varphi$ is defined as follows:

$$\boldsymbol{\tau}_\varphi=-\nu_\varphi\left(\nabla\mathbf{U}_\varphi+\nabla^{\mathrm{T}}\mathbf{U}_\varphi\right)+\frac{2}{3}\nu_\varphi\nabla\cdot(\mathbf{U}_\varphi\cdot\mathbf{I}), \tag{5}$$

where ν_φ is the molecular kinematic viscosity and $\mathbf{I}$ is the identity matrix. According to the Boussinesq eddy viscosity concept, $\mathbf{R}_\varphi$ in Eqs. (3) and (4) is given as

$$\mathbf{R}_\varphi=-\nu_{\varphi,t}\left(\nabla\mathbf{U}_\varphi+\nabla^{\mathrm{T}}\mathbf{U}_\varphi\right)+\frac{2}{3}\nu_{\varphi,t}\nabla\cdot(\mathbf{U}_\varphi\cdot\mathbf{I})+\frac{2}{3}k_\varphi\mathbf{I}, \tag{6}$$

where k_φ is the turbulent kinetic energy and $\nu_{\varphi,t}$ is the phase turbulent viscosity, which need to be calculated from the turbulence model. The interfacial force exchange term $\mathbf{M}$ describes the momentum exchange between the two phases and requires a certain degree of modeling. It is common to break it down into the axial drag force $\mathbf{M}_{\mathrm{drag}}$; the lateral lift force $\mathbf{M}_{\mathrm{lift}}$, which acts perpendicular to the direction of the relative motion of the two phases (Tomiyama et al., 2002); the virtual mass force $\mathbf{M}_{\mathrm{vm}}$, which is proportional to relative phase accelerations (Lamb, 1932); the wall lubrication force $\mathbf{M}_{\mathrm{wall}}$ which acts to drive the bubble away from the wall (Antal et al., 1991); and the turbulent dispersion force $\mathbf{M}_{\mathrm{turb}}$, which is the result of the turbulent fluctuations of the liquid velocity (De Bertodano, 1992). Specifically, the drag force can be calculated as follows:

$$\mathbf{M}_{\mathrm{drag}}=\frac{3}{4}\alpha_a\rho_b C_D\frac{1}{d_a}|\mathbf{U}_r|\mathbf{U}_r, \tag{7}$$

where C_D is the drag force coefficient and d_a is the diameter of phase a. The lift force can be calculated as follows:

$$\mathbf{M}_{\mathrm{lift}}=\alpha_a C_L\rho_b\mathbf{U}_r\times(\nabla\times\mathbf{U}_b) \tag{8}$$

where C_L is the lift force coefficient. The virtual mass force can be calculated as follows:

$$\mathbf{M}_{\mathrm{vm}}=\alpha_a C_{\mathrm{vm}}\rho_b\left(\frac{\mathrm{D}\mathbf{U}_b}{\mathrm{D}t}-\frac{\mathrm{D}\mathbf{U}_a}{\mathrm{D}t}\right) \tag{9}$$

where C_{vm} is the virtual mass force coefficient. In this work, only the drag force was investigated as it dominates the terminal rise velocity of the bubbles (Díaz et al., 2008; Roghair et al., 2011). The modeling of the drag force is discussed in more detail in Section 3.

Although the governing equations reported for TFM are well organized, it is still well known that they possess complex characteristics and exhibit instabilities (Park et al., 1999; Vaidheeswaran and Lopez De Bertodano, 2017), and it is usually not possible to achieve a physical solution if they are solved directly. The first problem is that the phase momentum equations become singular when α_a or α_b tends to be null (Oliveira and Issa, 2003; Weller, 2002), which is a frequent situation for separated flows. Another problem is the adequate treatment of the drag force to ensure the robustness of the algorithm and predict reasonable results. In the following, the different numerical re-formulations are discussed to address these problems.

2.1. Non-conservative phase momentum equations

Two possible solutions to deal with the singular problems were proposed by Weller (2002). One solution is to limit α such that $\alpha\to\delta$, where $0<\delta\ll1$; the other solution is to force $\lim_{\alpha\to0}\mathbf{U}=\mathbf{U}^*$, where the value of $\mathbf{U}^*$ is obtained from a model. However, none of these approaches is satisfactory. The problem for the first approach is related to a conservation issue. The numerical treatment should ensure local and global conservation, especially when a finite volume method is applied. If the singular problem is prevented by limiting α to a certain threshold value (e.g., 0.001), the global conservation of the phase fraction cannot be ensured. For example, for a single-phase flow, where no dispersed phase exists, the global dispersed phase fraction should be exactly zero. However, the approach has to limit the dispersed phase fraction to a small value, which violates the global conservation. This conservation violation will pose a problem, especially for those liquid-liquid test cases where a rather dilute system is investigated (Gao et al., 2016). The second issue is that, by forcing the phase velocity to be a certain value, such a model introduces randomness into the results. Instead of solving the standard phase momentum equations (Eqs. (3) and (4)) directly, dividing the phase momentum equations by the phase fraction leads to well-behaved phase velocity fields in the limit of the other phase vanishing (Oliveira and Issa, 2003). For incompressible flows, after some

mathematical rearrangements, the phase momentum equation for phase a is reported as follows:

$$\frac{\partial \mathbf{U}_a}{\partial t} + \mathbf{U}_a \cdot \nabla \mathbf{U}_a + \frac{\nabla \alpha_a \rho_a}{\alpha_a \rho_a} \cdot \left(\mathbf{R}_{\mathrm{eff},a}\right) + \nabla \cdot \mathbf{R}_{\mathrm{eff},a} = -\frac{\nabla p}{\rho_a} + \mathbf{g} - \frac{\mathbf{M}}{\alpha_a \rho_a}, \tag{10}$$

where $\mathbf{R}_{\mathrm{eff},a} = \boldsymbol{\tau}_a + \mathbf{R}_a$. The phase momentum equation for phase b is neglected here as it has a the same general form. The feature of Eq. (10) is that it transforms the original conservative phase momentum equations to a non-conservative form, which might induce some numerical errors. However, the advantage of the non-conservative phase momentum equation formulations is that they allow the equations to be solved in the entire computational domain instead of manually setting the velocity to be some value. The non-conservative phase momentum equations were implemented in `bubbleFoam` in OpenFOAM-1.7.1, and these are addressed using the so-called phase-intensive formulations.

2.2. Semi-conservative and fully conservative phase momentum equations

Many test cases have shown that the numerical modeling of the non-conservative phase momentum equations is accurate for some flows (e.g., sudden expansion flow) (Oliveira and Issa, 2003; Rusche, 2003) in which the pressure difference is not large over the computational domain and that it is only valid for incompressible multiphase flows. However, the compressibility effect is very important in many two-phase systems, in particular in bubble columns, in which the pressure difference from top to bottom may be significant: this pressure difference makes the bubble size at the bottom smaller than that at the top. Moreover, it can further generate a source term in phase fraction equations, which explain the phase fraction variation due to the pressure difference. However, the density variations within each phase are typically quite small compared with the density difference between the phases (Weller, 2002; Cano-Pleite et al., 2015). On the basis of this assumption, we can derive the semi-conservative phase momentum equations and write the phase momentum equation for phase a as

$$\alpha_a \rho_a \frac{\partial \mathbf{U}_a}{\partial t} + \alpha_a \rho_a \mathbf{U}_a \nabla \cdot \mathbf{U}_a + \nabla \cdot \left(\alpha_a \rho_a \mathbf{R}_{\mathrm{eff},a}\right) = -\alpha_a \nabla p + \alpha_a \rho_a \mathbf{g} - \mathbf{M}. \tag{11}$$

If we divide out ρ_a in both sides of Eq. (11), it becomes

$$\alpha_a \frac{\partial \mathbf{U}_a}{\partial t} + \alpha_a \mathbf{U}_a \nabla \cdot \mathbf{U}_a + \nabla \cdot \left(\alpha_a \mathbf{R}_{\mathrm{eff},a}\right) = -\frac{\alpha_a}{\rho_a} \nabla p + \alpha_a \mathbf{g} - \frac{\mathbf{M}}{\rho_a}. \tag{12}$$

It can be seen that Eq. (12) features no diffusive flux that can be discretized implicitly. However, the finite volume scheme that any CFD code uses to discretize the equations generates a numerical diffusion. $\mathbf{R}_{\mathrm{eff,d}}$ is therefore broken down into two contributions for numerical considerations (Weller, 2002; Rusche, 2003):

$$\begin{aligned}\mathbf{R}_{\mathrm{eff},a} &= \mathbf{R}_{\mathrm{eff},a} + \nu_{\mathrm{eff},a} \nabla \mathbf{U}_a - \nu_{\mathrm{eff},a} \nabla \mathbf{U}_a \\ &= -\nu_{\mathrm{eff},a}\left(\nabla \mathbf{U} + \nabla^{\mathrm{T}} \mathbf{U}_a\right) + \frac{2}{3} \nu_{\mathrm{eff},a} \mathbf{I} \nabla \cdot \mathbf{U}_a + \frac{2}{3} \mathbf{I} k_a \\ &\quad + \nu_{\mathrm{eff},a} \nabla \mathbf{U}_a - \nu_{\mathrm{eff},a} \nabla \mathbf{U}_a \\ &= \left(-\nu_{\mathrm{eff},a} \nabla^{\mathrm{T}} \mathbf{U}_a + \frac{2}{3} \nu_{\mathrm{eff},a} \mathbf{I} \nabla \cdot \mathbf{U}_a + \frac{2}{3} k_a \mathbf{I}\right) - \nu_{\mathrm{eff},a} \nabla \mathbf{U}_a \\ &= \mathbf{R}^{\mathrm{c}}_{\mathrm{eff},a} - \nu_{\mathrm{eff},a} \nabla \mathbf{U}_a.\end{aligned} \tag{13}$$

Then, the third term in Eq. (12) can be replaced by $\nabla \cdot \mathbf{R}^{\mathrm{c}}_{\mathrm{eff},a} - \nabla \cdot \left(\alpha_a \nu_{\mathrm{eff},a} \nabla \mathbf{U}_a\right)$. The diffusive terms with respect to $\mathbf{U}_a$ are artificially introduced and can be discretized implicitly to decrease the numerical diffusion. Moreover, for numerical reasons, the terms $\alpha_a \frac{\partial \mathbf{U}_a}{\partial t}$ and $\alpha_a \mathbf{U}_a \cdot \nabla \mathbf{U}_a$ in Eq. (12) are usually replaced by a conservative convection term minus a divergence term because it helps maintain the boundedness of the solution variable and promotes better convergence. They can be reformulated as follows:

$$\alpha_a \mathbf{U}_a \cdot \nabla \mathbf{U}_a = \nabla \cdot \left(\alpha_a \mathbf{U}_a \mathbf{U}_a\right) - \mathbf{U}_a \nabla \cdot \alpha_a \mathbf{U}_a, \tag{14}$$

$$\alpha_a \frac{\partial \mathbf{U}_a}{\partial t} = \frac{\partial \left(\alpha_a \mathbf{U}_a\right)}{\partial t} - \mathbf{U}_a \frac{\partial \alpha_a}{\partial t}. \tag{15}$$

By substituting Eqs. (13)–(15) into Eq. (12), we can write the corresponding discretized semi-conservative phase momentum equation for phase a as

$$\frac{\partial \left(\alpha_a \lfloor \mathbf{U}_a \rfloor\right)}{\partial t} + \nabla \cdot \left(\alpha_a \mathbf{U}_a \lfloor \mathbf{U}_a \rfloor\right) - \left(\nabla \cdot \alpha_a \mathbf{U}_a + \frac{\partial \alpha_a}{\partial t}\right) \mathbf{U}_a + \nabla \cdot \left(\alpha_a \mathbf{R}^{\mathrm{c}}_{\mathrm{eff},a}\right) - \nabla \cdot \left(\alpha_a \nu_{\mathrm{eff},a} \nabla \lfloor \mathbf{U}_a \rfloor\right) = -\frac{\mathbf{M}}{\rho_a}. \tag{16}$$

where $\lfloor \rfloor$ means implicit discretization. In the spirit of the Rhie-Chow interpolation (Rhie and Chow, 1983), to prevent pressure oscillations, Eq. (16) does not include the contribution from the pressure and it only provides a first prediction of the phase velocity, which needs to be corrected after the pressure is updated. The buoyant force term, $\mathbf{g}$, is not included either as it is proven that the body force is better included in the pressure Poisson equation as well (Zhang et al., 2014). The terms with respect to $\mathbf{U}_a$ in Eq. (16) are discretized implicitly; the others are discretized explicitly (e.g., $\nabla \cdot \left(\alpha_a \mathbf{R}^{\mathrm{c}}_{\mathrm{eff},a}\right)$). The discretized semi-conservative phase momentum equation for phase b can be derived by the same approach. After the phase velocity is predicted, there are different ways to link the drag force and the other force terms to the phase velocity (Oliveira and Issa, 1994). In this work, the partial elimination method was adopted, which was developed originally by Spalding (1980). It has the advantage of decoupling each phase velocity from its complementary phase, which favors the momentum convergence for drag-dominated problems. Other techniques can also be used, such as the partial elimination method (PIM) (Karema and Lo, 1999); a comparison of these different methods can be found in the literature (Miller and Miller, 2003).

For the fully conservative formulations, the derivation is neglected here for simplicity. Only the discretized phase momentum equation for phase a is reported here, which is formulated as follows:

$$\frac{\partial \left(\alpha_a \rho_a \lfloor \mathbf{U}_a \rfloor\right)}{\partial t} + \nabla \cdot \left(\alpha_a \rho_a \mathbf{U}_a \lfloor \mathbf{U}_a \rfloor\right) - \left(\nabla \cdot \alpha_a \rho_a \mathbf{U}_a + \frac{\partial \alpha_a \rho_a}{\partial t}\right) \mathbf{U}_a + \nabla \cdot \left(\alpha_a \rho_a \mathbf{R}^{\mathrm{c}}_{\mathrm{eff},a}\right) - \nabla \cdot \left(\alpha_a \mu_{\mathrm{eff},a} \nabla \lfloor \mathbf{U}_a \rfloor\right) = -\mathbf{M}. \tag{17}$$

2.3. Pressure Poisson equations

Solving Eqs. (16) or (17) gives the predicted phase velocity for phase a and phase b, which do not satisfy the continuity constraint. Hence, a pressure Poisson equation should be formulated to correct the flux. If only the drag force is included, before the pressure Poisson equation is constructed, the contribution from the pressure gradient, the gravity acceleration vector, and the contribution from the explicit drag force should be grouped together to update the phase velocity. For the semi-conservative formulations, the predicted phase velocity reads as

$$\mathbf{U}_a = \mathrm{HbyA}_a - \frac{1}{A_a}\left(\frac{\alpha_a \nabla p}{\rho_a} - \alpha_a \mathbf{g} - \frac{\mathrm{Kd}}{\rho_a} |\mathbf{U}_r| \mathbf{U}_b\right), \tag{18}$$

$$\mathbf{U}_b = \mathrm{HbyA}_b - \frac{1}{A_b}\left(\frac{\alpha_b \nabla p}{\rho_b} - \alpha_b \mathbf{g} - \frac{\mathrm{Kd}}{\rho_b} |\mathbf{U}_r| \mathbf{U}_a\right), \tag{19}$$

where HbyA stands for the finite volume representation of the spatial convective and diffusive fluxes of the phase momentum (Issa et al., 1986). If phase a is assumed to be dispersed, Kd can be calculated by

$$\mathrm{Kd} = \frac{3}{4}\alpha_a C_D \frac{\rho_b}{d_a}. \tag{20}$$

It should be noted here that the right-hand side of Eqs. (18) and (19) was divided by the phase density in the semi-conservative formulations. However, the phase density should be kept in the fully conservative formulations. If Eqs. (1) and (2) were written to be non-conservative, they could be expressed as follows:

$$\frac{\partial \alpha_a}{\partial t} + \nabla\cdot(\alpha_a \mathbf{U}_a) = -\frac{\alpha_a}{\rho_a}\frac{\mathrm{D}\rho_a}{\mathrm{D}t}, \tag{21}$$

$$\frac{\partial \alpha_b}{\partial t} + \nabla\cdot(\alpha_b \mathbf{U}_b) = -\frac{\alpha_b}{\rho_b}\frac{\mathrm{D}\rho_b}{\mathrm{D}t}. \tag{22}$$

Summarizing Eqs. (21) and (22) together produces the compressibility constraint equation:

$$\nabla\cdot\mathbf{U} = \nabla\cdot(\alpha_a\mathbf{U}_a + \alpha_b\mathbf{U}_b) = -\frac{\alpha_a}{\rho_a}\frac{\mathrm{D}\rho_a}{\mathrm{D}t} - \frac{\alpha_b}{\rho_b}\frac{\mathrm{D}\rho_b}{\mathrm{D}t}. \tag{23}$$

It can be seen that, in contrast with the incompressible two-phase flows, the velocity field of the compressible flows is not divergence free. Substituting Eqs. (18) and (19) into Eq. (23), we can construct the compressible pressure Poisson equation as follows:

$$\begin{aligned}
&\nabla\cdot\left(\left(\alpha_a\frac{\alpha_a}{A_a\rho_a} + \alpha_b\frac{\alpha_b}{A_b\rho_b}\right)\nabla p\right)\\
&= \nabla\cdot\left(\alpha_a\left(\mathrm{HbyA}_a + \frac{\alpha_a\mathbf{g}}{A_a} + \frac{\mathrm{Kd}}{A_a\rho_a}|\mathbf{U}_r|\mathbf{U}_a\right)\right.\\
&\quad\left.+\alpha_b\left(\mathrm{HbyA}_b + \frac{\alpha_b\mathbf{g}}{A_b} + \frac{\mathrm{Kd}}{A_b\rho_b}|\mathbf{U}_r|\mathbf{U}_b\right)\right) + \left(\frac{\alpha_a}{\rho_a}\frac{\mathrm{D}\rho_a}{\mathrm{D}t} + \frac{\alpha_b}{\rho_b}\frac{\mathrm{D}\rho_b}{\mathrm{D}t}\right).
\end{aligned} \tag{24}$$

It can be seen that Eq. (24) is different from the basic pressure Poisson equation. This difference is motivated by numerical stability considerations. OpenFOAM adopts a co-located grid arrangement, storing all variables at cell centroids, with the exception of boundary values, which are stored at the centroid of each boundary face. With such an arrangement, the Rhie-Chow interpolation is used to avoid pressure checker-boarding (Rhie and Chow, 1983). In the spirit of the Rhie and Chow procedure, the pressure gradient term is not discretized in Eq. (13). Moreover, the standard Rhie-Chow procedure exhibits difficulties when a large body force exists (Zhang et al., 2014). It is better to move the buoyant force term $\mathbf{g}$ and the explicit drag force term into the pressure Poisson equation. Moreover, whether the interphase force term is presented in the pressure Poisson equation is determined by the phase momentum discretization and Rhie-Chow interpolation. If the force term is expressed as a function of the velocity of phase a, it can be included into the momentum equation of phase a and it should be discretized implicitly. A similar methodology can be applied to other interphase force terms (e.g. the lift force).

2.4. Compressible phase fraction equation

When solving the phase fraction equations, the key issue is to ensure the boundedness of the phase fraction as unbounded solutions may look reasonable but are totally wrong. The use of upwind approximation can guarantee that the phase fraction is bounded by zero, but it cannot guarantee that it is bounded by one. If the phase equations for both phases are solved together and an appropriate bounded discretization scheme is applied, $\alpha \geqslant 0$ and the constraint $\alpha \leqslant 1$ will be obeyed (Oliveira and Issa, 2003). However, this method does not guarantee conservation, which is a critical issue in multiphase flows with high density ratios because small phase fraction errors may correspond to large mass-fraction errors. Weller (2002) proposed breaking down $\mathbf{U}_a$ into the mean and relative parts:

$$\mathbf{U}_a = \mathbf{U} + \alpha_a\mathbf{U}_r. \tag{25}$$

Substituting Eq. (25) into Eq. (1) and dividing by the dispersed phase density, we can write the dispersed phase fraction equation for the incompressible flows as

$$\frac{\partial \alpha_a}{\partial t} + \nabla\cdot(\mathbf{U}\alpha_a) + \nabla\cdot(\mathbf{U}_r\alpha_a\alpha_b) = 0. \tag{26}$$

In the compressible TFM, Eq. (26) is employed to calculate the dispersed phase fraction and the continuous phase fraction can be calculated by $\alpha_b = 1 - \alpha_a$. An interesting and useful feature of this reformulation is that the continuous phase equations have the same form as reported in Eq. (27).

$$\frac{\partial \alpha_b}{\partial t} + \nabla\cdot(\mathbf{U}\alpha_b) - \nabla\cdot(\mathbf{U}_r\alpha_a\alpha_b) = 0. \tag{27}$$

It can be seen in Eq. (26) that the second term on the left hand side does indeed have a convection velocity $\mathbf{U}$ applicable for both phases. However, the third term on the left hand side has a convection velocity of either $\mathbf{U}_r$ or $-\mathbf{U}_r$. Considering a first order upwind and downwind scheme, the interpolation manipulation corresponds exactly to the high resolution interface capturing (HRIC) scheme (Muzaferija and Perić, 1997), which was developed to ensure conservation and boundedness based on the normalized variable diagram (NVD). When Eq. (26) was solved, the first convection term is conservative and $0 \leqslant \alpha_a \leqslant 1$ because $\nabla\cdot\mathbf{U} = 0$. The second convection term in Eq. (26) can also be conservative and $0 \leqslant \alpha_a \leqslant 1$ if the convection scheme of $\mathbf{U}_r$ is used to interpolate α_a in the cell face and the convection scheme of $-\mathbf{U}_r$ is used to interpolate α_b in the cell face following the HRIC scheme spirit. Although this treatment is quite diffusive if an upwind scheme is employed, it can ensure the boundedness of the solution. A higher-order differencing scheme can reduce the numerical diffusion but will compromise the boundedness (Rusche, 2003).

Following the similar arrangement in Eqs. (26), (21) in the compressible phase, we can write the equation as

$$\frac{\partial \alpha_a}{\partial t} + \nabla\cdot(\mathbf{U}\alpha_a) + \nabla\cdot(\mathbf{U}_r\alpha_a(1-\alpha_a)) = -\frac{\alpha_a}{\rho_a}\frac{\mathrm{D}\rho_a}{\mathrm{D}t}. \tag{28}$$

However, unlike the case of the incompressible flows, if Eq. (28) is solved directly, the boundedness cannot be guaranteed again because $\nabla\cdot(\mathbf{U}\alpha_a) = \mathbf{U}\cdot\nabla\alpha_a + \alpha_a\nabla\cdot\mathbf{U}$ contains a non-vanishing term $\nabla\cdot\mathbf{U}$, which acts as a source or sink, depending on the sign of $\nabla\cdot\mathbf{U}$. This term is not zero when either phase fraction approaches zero. This problem can be handled by simply breaking down $\nabla\cdot(\mathbf{U}\alpha_a)$ and substituting Eq. (21) into Eq. (28):

$$\frac{\partial \alpha_a}{\partial t} + \mathbf{U}\cdot\nabla\alpha_a + \nabla\cdot(\mathbf{U}_r\alpha_a(1-\alpha_a)) = \alpha_a\alpha_b\left(\frac{1}{\rho_b}\frac{\mathrm{D}\rho_b}{\mathrm{D}t} - \frac{1}{\rho_a}\frac{\mathrm{D}\rho_a}{\mathrm{D}t}\right) \tag{29}$$

$$\frac{\partial \alpha_a}{\partial t} + \nabla\cdot(\alpha_a\mathbf{U}) + \nabla\cdot(\mathbf{U}_r\alpha_a(1-\alpha_a)) = \alpha_a\alpha_b\mathrm{dgdt} + \alpha_a\nabla\cdot\mathbf{U} \tag{30}$$

where $\mathrm{dgdt} = \left(\frac{1}{\rho_b}\frac{\mathrm{D}\rho_b}{\mathrm{D}t} - \frac{1}{\rho_a}\frac{\mathrm{D}\rho_a}{\mathrm{D}t}\right)$. Eq. (30) will ensure the boundedness of the phase fraction as the right-hand side of it becomes zero when either phase fraction is zero.

2.5. Two-phase turbulence model

Eqs. (3) and (4) require closure relations for the Reynolds stress, $\mathbf{R}_{\varphi}$, which arises in the momentum equations as a result of the averaging process. These unknown stresses represent the effects of turbulence on the average phase momentum and need to be expressed in terms of known quantities for closure. The single-phase $k-\varepsilon$ turbulence model was found to offer a good trade-off between accuracy and computational costs compared with the two-phase Reynolds stress turbulence models (Hanjalic and Launder, 1972; Lopez De Bertodano et al., 1990), and it has been employed in many studies for two-phase flows (Petitti et al., 2013; Alopaeus et al., 2002). However, in our preliminary investigation, the magnitude of the vertical liquid velocity predicted by the single-phase $k-\varepsilon$ model was not good enough compared with the experimental data, although the plume oscillation period (POP) was predicted well. In this study, a two-phase $k-\varepsilon$ model (Sharma et al., 2017; Bhusare et al., 2017) was employed. Furthermore, a source term was included into the k equation and ε equation of the liquid phase to introduce the bubble-induced turbulence (Lahey, 1990).

It has been shown by Lopez De Bertodano et al. (1994) that the single-phase $k-\varepsilon$ turbulence model (Launder and Spalding, 1974) can be extended to two-phase flows. The equations of the two-phase $k-\varepsilon$ model for phase a are reported as follows (Lahey, 2005):

$$\frac{\partial(\alpha_a\rho_a k_a)}{\partial t}+\nabla\cdot(\alpha_a\rho_a\mathbf{U}_a k_a)-\nabla\cdot(\alpha_k\rho_a\nu_{a,t}\nabla k_a)=\alpha_a G-\alpha_a\rho_a\varepsilon_a, \tag{31}$$

$$\frac{\partial(\alpha_a\rho_a\varepsilon_a)}{\partial t}+\nabla\cdot(\alpha_a\rho_a\mathbf{U}_a\varepsilon_a)-\nabla\cdot(\alpha_\varepsilon\rho_a\nu_{a,t}\nabla\varepsilon_a)=C_1\alpha_a G\frac{\varepsilon_a}{k_a}-C_2\alpha_a\rho_a\frac{\varepsilon_a}{k_a}\varepsilon_a-C_3\alpha_a\rho_a\nabla\cdot(\mathbf{U}\cdot\mathbf{I}), \tag{32}$$

where G is the production of the turbulent kinetic energy, which can be expressed as follows:

$$G=2\nu_{a,t}\rho_a\left(\mathbf{S}:\mathbf{S}-\frac{2}{3}\mathrm{tr}(\mathbf{S})^2\cdot\mathbf{I}\right)+\frac{2}{3}\rho_a k_a\nabla\cdot(\mathbf{U}\cdot\mathbf{I}), \tag{33}$$

where $\mathbf{S}=\nabla\mathbf{U}_a+\nabla\mathbf{U}_a^{\mathrm{T}}$. C_1, C_2, and C_3 are the $k-\varepsilon$ model parameters ($C_1=1.44, C_2=1.92$, and $C_3=0.33$), and α_k and α_ε are the turbulent Schmidt number for k and ε, respectively ($\alpha_k=1.0, \alpha_\varepsilon=0.76923$). $\nu_{a,t}$ is the turbulent viscosity of the continuous phase. In the single-phase $k-\varepsilon$ model, it can be calculated by $\nu_{a,t}=C_t^2\nu_{b,t}$. C_t is the turbulent response coefficient (Gosman et al., 1992), which is defined as the ratio of the dispersed phase velocity fluctuations to those of the continuous phase. The liquid velocity is very sensitive to this value as it scales the effective viscosity. In OpenFOAM-4.0, a new model was employed to calculate the response coefficient, which has never been tested in the literature. The response coefficient is calculated from the turbulent time scale by

$$C_t=\frac{1-\theta}{1+\theta}, \tag{34}$$

where $\theta=\min\left(\exp\left(\min\left(\theta_l/\theta_g,50\right)\right),1\right)$. The turbulent time scale is calculated as follows:

$$\theta_l=\frac{k_b}{\varepsilon_b}, \tag{35}$$

$$\theta_g=\frac{1}{18\mu_b}\rho_b d_a^2. \tag{36}$$

More information about the effect of the response coefficient on the flow fields can be found in Zhang et al. (2006).It should be mentioned here that the two-phase equations reported in Eqs. (31) and (32) can be used for compressible flows and that the last term of Eq. (32) is the so-called Reynolds deduced turbulence (RDT) term (El Tahry, 1983). For incompressible flows, the RDT term equals zero.

The k and ε equations for phase b are not reported here for simplicity. The only difference is that the effective viscosity for phase b is calculated by $\nu_{b,t}=C_\mu\frac{k_b^2}{\varepsilon_b}$, where C_μ is the $k-\varepsilon$ model parameter, which is equal to 0.09. It should be stressed here that bubble-induced turbulence should be introduced into the continuous phase equations, and it is reported as follows (Lahey, 2005):

$$S=\alpha_b\rho_b C_p\left(1+C_{D,a}^{4/3}\right)\frac{|\mathbf{U}_r|^3}{d_a} \tag{37}$$

where $C_p=0.25$ for the potential flow around a sphere (Arnold et al., 1989). It accounts for the velocity fluctuations induced by the liquid displacement due to the relative velocity and the liquid eddies that may be formed behind the bubbles.

3. Numerical treatments for the two-fluid model

The singular problems for the semi-conservative and fully conservative phase momentum equations and the two-phase $k-\varepsilon$ model can be handled by special numerical treatments. Below, we start with the phase momentum equations, and then, we present the turbulent equations.

In most of the cases, the drag force plays the most important role in these five forces for bubbly flows (Díaz et al., 2008; Roghair et al., 2011). If phase a is assumed to be dispersed, it is common to calculate the drag force in the whole computational domain from the following equation (Ishii and Zuber, 1979):

$$\mathbf{M}_{\mathrm{drag}}=\frac{3}{4}\alpha_a\rho_b C_D\frac{1}{d_a}|\mathbf{U}_r|\mathbf{U}_r, \tag{38}$$

where d_a is the diameter of the dispersed phase (e.g., diameter of the bubbles for gas-liquid dispersions or diameter of the droplets for liquid-liquid dispersions); $\mathbf{U}_r$ is the relative velocity, which is equal to $\mathbf{U}_a-\mathbf{U}_b$; and C_D is the drag coefficient, which is usually determined empirically and depends on the properties of the dispersed phase. In this work, the drag coefficient correction by Grace et al. (1976) was implemented for the gas phase and that by Ishii and Zuber (1979) was implemented for the liquid phase. Further details about the different drag coefficient corrections were listed by Hjertager (1998) and Jakobsen et al. (1997).

However, when Eq. (38) is used as a sub-model of TFM, special treatments are needed. First, it can be seen that the singular problem exists in both the semi-conservative and the fully conservative phase momentum equations as reported in Eq. (16) and (17) when the phase fraction tends to be zero in some computational regions. This phenomenon is usually denoted as "phase segregation." The singular problem does not exist in the non-conservative phase momentum equations as the phase fraction is divided from the phase momentum equations (see Eq. (10)). However, another problematic term remains; it can be seen in Eq. (10) that the interfacial term, which is proportional to $\frac{\nabla\alpha_d}{\alpha_d}$, requires the gradient of α_d to go to zero faster than α_d, when $\alpha_d\to 0$. Usually, it is treated numerically to ensure that divisions by zero are avoided, allowing the non-conservative phase momentum equations to be solved throughout the whole computational domain (Passalacqua and Fox, 2011).

For the semi-conservative and fully conservative phase momentum equations, this singular problem may also be avoided by setting the dispersed phase velocity equal to the velocity of the continuous phase in those cells where the dispersed phase fraction

is below a certain critical value. As the drag force term cannot be neglected in most of the cases, a natural way to achieve this is to preserve the drag force as a non-zero term in the phase momentum equations when the phase fraction tends to zero. The drag force reported in Eq. (38) can be slightly modified as follows

$$\mathbf{M}_{\text{drag}} = \frac{3}{4}\max(\alpha_{\text{a}}, \alpha_s)\rho_{\text{b}} C_{\text{D}} \frac{1}{d_{\text{a}}}|\mathbf{U}_{\text{r}}|\mathbf{U}_{\text{r}}, \tag{39}$$

where α_s is a small user-defined value (e.g., 0.0001). When the value of the dispersed phase is smaller than the user-defined value, in such circumstances, the phase momentum equation degenerates into a simple algebraic phase velocity equation. For example, the result of the degenerated dispersed phase momentum equation is $\mathbf{U}_{\text{a}} = \mathbf{U}_{\text{b}}$ and the relative velocity should be zero. This approach is also physically correct as the dispersed phase velocity of course tends to the same velocity of the continuous phase when the dispersed phase disappears.

A similar numerical treatment can also be applied to the turbulent equations as it can be seen that the singular problem also exists in the two-phase $k-\varepsilon$ model. A source term can be added to the k equation for phase b, which can be written as

$$S_{k,\text{b}} = \max(\alpha_{\text{b}}, \alpha_s)\rho_{\text{b}}(k_{\text{a}} - k_{\text{b}}), \tag{40}$$

$$S_{\varepsilon,\text{b}} = \max(\alpha_{\text{b}}, \alpha_s)\rho_{\text{b}}(\varepsilon_{\text{a}} - \varepsilon_{\text{b}}). \tag{41}$$

It can be seen that, when the value of phase b is lower than that of α_s, the turbulent fields of phase b are the same as those of phase a. The numerical treatments discussed above are quite effective for two-phase flows when phase segregation exists.

Another problem arises when phase inversion occurs, which is a prominent phenomenon, especially for liquid-liquid dispersions, as the difference in fluid properties in both phases is not notable. When phase inversion exists in some regions, the originally dispersed phase becomes the continuous phase and vice versa. This is not considered in the traditional drag force model reported in Eq. (38) or Eq. (39), which is formulated by assuming that phase a is always dispersed in phase b. However, in the computational regions where $\alpha_{\text{a}} \to 1$, phase b is dispersed in phase a. In such cases, a different particle diameter should be used in the drag force term.

In the blended methods implemented in OpenFOAM-4.0, the drag force is divided into two contributions: one from phase a and the other from phase b. It depends on the dispersed fraction parameter whether phase a and phase b can be inverted. The drag force can be calculated as follows:

$$\mathbf{M}_{\text{drag}} = (1 - f_a)\mathbf{M}_{\text{drag,a}} + f_b\mathbf{M}_{\text{drag,b}}, \tag{42}$$

where f_a and f_b are the blending coefficients and $\mathbf{M}_{\text{drag,a}}$ and $\mathbf{M}_{\text{drag,b}}$ are the corresponding drag force calculated on the basis of phase a and phase b. Eq. (42) can be further extended to include the contribution from both phases penetrating each other. The key essence of the blending approach is the calculation of the blending coefficients based on the phase fraction. In the linear blending method, the blending coefficients are calculated as follows:

$$f_a = \min\left(\max\left(\frac{\alpha_a - \alpha_{a,\text{F}}}{\alpha_{a,\text{P}} - \alpha_{a,\text{F}}}, 0\right), 1\right), \tag{43}$$

$$f_b = \min\left(\max\left(\frac{\alpha_{b,\text{P}} - \alpha_b}{\alpha_{b,\text{P}} - \alpha_{b,\text{F}}}, 0\right), 1\right), \tag{44}$$

where $\alpha_{a,\text{F}}$ and $\alpha_{b,\text{F}}$ are the maximum dispersed phase fraction for phase a and phase b, and $\alpha_{a,\text{P}}$ and $\alpha_{b,\text{P}}$ are the partly dispersed phase fraction for phase a and phase b, respectively. These parameters should be given in different cases. It can be seen that, if $\alpha_a = 0$, both f_a and f_b are equal to 0 and $\mathbf{M}_{\text{drag}} = \mathbf{M}_{\text{drag,a}}$, which means that the drag force should be calculated from phase a independently. In contrast, when $\alpha_a = 1$, the drag force should be calculated from phase b. In the hyperbolic blending method, the blending coefficients are calculated as follows:

$$f_a = \frac{1 + \tanh\left(\frac{4}{B_a}(\alpha_a - \alpha_{a,\text{F}})\right)}{2}, \tag{45}$$

$$f_b = \frac{1 + \tanh\left(\frac{4}{B_b}(\alpha_{b,\text{F}} - \alpha_b)\right)}{2}, \tag{46}$$

where B_a and B_b define the phase transition range. Again, these parameters, together with $\alpha_{a,\text{F}}$ and $\alpha_{b,\text{F}}$, should be set by the user in different cases. The blending method can be applied not only to the semi-conservative and the fully conservative formulations of TFM, but also to the non-conservative formulations. Although the singular problem is circumvented in the non-conservative formulations, the feasible calculation of the interphase transfer terms still remains an issue when a phase inversion phenomenon occurs. Furthermore, this type of blending method can also be used for the formulation in the volume-of-fraction (VOF) method (Höhne and Mehlhoop, 2014).

4. Test case and numerical details

For the validation of the numerical treatments mentioned above, the three-dimensional test case studied here was that of a turbulent bubbly flow in a bubble column, experiments on which were carried out by Díaz et al. (2008). Although this column configuration is simple, it has been proven to be a very interesting test case because the liquid vortices generated by the bubble plumes are a favorable factor for mixing and, therefore, for speeding up all transport processes (Sokolichin et al., 1997). Additionally, the existence of flow structures showing unsteady liquid recirculation is a typical phenomenon in industrial-scale bubble columns. The experimental setup included a 0.2-m-wide, 1.8-m-high, and 0.04-m-deep bubble column (Díaz et al., 2008). The column was filled with water (H = 0.45 m) at room temperature and atmospheric pressure, whereas air was fed with different velocities from the gas chamber through a sparger (eight centered holes of 0.001 m in diameter and 0.006 m in pitch).

The height of the grid reported in the work of Díaz et al. (2008) was the same as that of the water, which was equal to 0.45 m, and no phase segregation occurred. To test the capability of the TFM to simulate turbulent bubbly flows in case of phase segregation, we extended the height of the computational mesh to 0.6 m (see Fig. 1). A fully orthogonal hexahedral grid with 40 (height) × 17 (width) × 7 (depth) cells was generated by `blockMesh`. Before

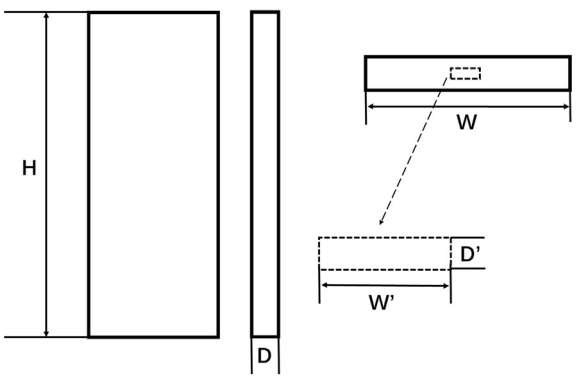

Fig. 1. Geometry of the bubble column investigated in this work: $H = 0.6$ m, $D = 0.04$ m, $W = 0.2$ m, $W\prime = 0.018$ m, and $D\prime = 0.006$ m. The inlet patch is marked by the dashed rectangle.

the simulations were performed, grid independence was investigated. We confirmed that the non-uniform hexahedral grids with 17 (width) × 7 (depth) × 40 (height) cells are enough to capture the plume oscillations, which are an essential phenomenon for the test case. Hence, this grid was selected for further work. Further information about the mesh independence investigation can been found in Díaz et al. (2008). The diameter of the bubbles entering the computational domain was set to 0.00505 m for the three-dimensional simulations, which is the same as in the literature (Díaz et al., 2008). The area of the sparger through which gas enters the domain was modeled as a rectangle with an area equal to the total areas, enclosed by the eight centered 0.001-m circular holes. This simplification was also employed in other works, and it has been proven to be efficient for meshing (Díaz et al., 2008; Buwa et al., 2006; Buffo et al., 2013b).

At the walls, a no-slip boundary condition for the liquid phase and a free-slip boundary condition for the gas phase were considered. The standard $k-\varepsilon$ wall functions were employed to calculate the turbulent viscosity near the wall. At the inlet, the velocity of the gas phase was calculated from the superficial velocity in different test cases; the turbulent intensity was assumed to be 0.05. In the preliminary tests, the turbulent intensity had little effect on the results after steady state was reached.

5. Results and discussions

5.1. Two-dimensional phase segregation simulations

Before discussing the results of the three-dimensional bubble column test case, a two-dimensional vertical plane 1 m in height and 1 m in width was used to simulate a conceptual phase segregation problem. A uniform 40 × 40 hex orthogonal mesh was used. Initially, the vertical plane was filled with a homogeneous air-water mixture with an air phase fraction of 0.5. At $t = 0$ s, the water was set in motion by gravity; the air phase went up and the water phase moved down. In a steady state, the phase segregation was completed and the interface of the air phase and water phase was formed in the middle of the vertical plane. A similar simulation was also investigated by Park et al. (2009) using another CFD code, as it is characterized by the existence of sharp density gradients at the lower and upper regions. Here, the difference between our work and that of Park et al. (2009) should be highlighted. In the latter work, only the results predicted by laminar simulations were compared with analytical solutions. However, singular problems do also arise when the two-phase $k-\varepsilon$ equations are employed, and this can be prevented effectively by the numerical treatment discussed in this paper. Furthermore, the simulations of Park et al. (2009) were performed using CUPID, which is rather different from our CFD code OpenFOAM. Such basic numerical investigations should be verified and compared with the analytical solutions before more realistic simulations are investigated in the following sections. The analytical solution for the phase segregation can be obtained by assuming quasi-steady-state flow conditions where the volumetric upward and downward fluxes of the two phases compensate each other (Stadtke, 2006). The comparison of the predicted air phase fraction at $x = 0.5$ m is reported in Fig. 2. It can be seen that both formulations predicted accurate results compared with the analytical solutions. The predicted phase fractions for air and water were also strictly bounded between 0 and 1. Further mesh refinement can make the results better as the interface becomes sharper.

5.2. Single-phase flows simulated by a two-phase solver

The results of the two-dimensional phase segregation test case in the previous section confirmed that the numerical treatment for the drag forces can prevent the singular problems while solving the semi-conservative and fully conservative phase momentum equations. In this section, we employed the two-phase solver to simulate a single-phase flow to investigate the capability of the numerical treatment for the source terms of the two-phase $k-\varepsilon$ model to prevent the singular problems. It should be noted here that the two-phase solver should behave as a single-phase solver when only one phase is present in the system. The geometry discussed in the previous section was modified to simulate a channel flow, for which the width was 0.06 m and the height was 1.0 m. The air was fed at the inlet of the channel, where a velocity of 0.1 m/s was specified. A two-dimensional orthogonal mesh was used with 25 nodes in width and 75 nodes in height. To compare with the analytical solution, we first launched the simulation by using a laminar model. The analytical solution for the fully developed channel laminar flow is reported as follows:

$$v = 0.15\, v_{\mathrm{IN}}\left(1 - \left(\frac{x}{0.03}\right)^2\right), \tag{47}$$

where v is the air velocity component in the height direction and x is the distance from the channel center. It can be seen from Fig. 3(a) that the velocity plots predicted by the semi-conservative and fully conservative formulations overlapped and did agree well with the analytical parabolic velocity profile. The simulation was further extended to include the two-phase $k-\varepsilon$ model. The turbulent energy dissipation rate for the air phase and the water phase predicted by the fully conservative formulation is reported in Fig. 3 (b). It can be seen that the turbulent energy dissipation rate for the water phase was identical to that of the air phase, which confirms that the numerical treatments reported in Eqs. (40) and (41) are effective in preventing the singular problems in the two-phase $k-\varepsilon$ model.

5.3. Investigation of the blending coefficients

Let us analyze the comparison between the blending coefficients predicted by the linear blending method and those by the hyperbolic blending method when different parameters are used. These plots are reported in Fig. 4. It can be seen that, in the linear blending method, the blending coefficient was 0 or 1 when the phase fraction was beyond the limit of $[\alpha_{a,\mathrm{F}}, \alpha_{a,\mathrm{P}}]$, which means that the drag force was calculated independently of one phase as, in such cases, phase a or phase b is considered to be fully dispersed. When the phase fraction's value is within the range of $[\alpha_{a,\mathrm{F}}, \alpha_{a,\mathrm{P}}]$, this phase fraction range can be seen as a phase transition range. In this range, the blending coefficients are not zero; the drag force is calculated from both phases. The width of the phase transition range is determined by the difference between $\alpha_{a,\mathrm{F}}$ and $\alpha_{a,\mathrm{P}}$. The smaller the difference, the smaller the phase transition range and the sharper the slope. Increasing the value of $\alpha_{a,\mathrm{F}}$ only shifts the plot horizontally. For the hyperbolic blending method, the larger the value of B, the wider the range of the phase transition. The value of $\alpha_{a,\mathrm{F}}$ is located in the middle of the phase transition range. Furthermore, it can be seen that the shape of the hyperbolic blending method was smoother than the linear blending method. Meanwhile, the only difference between the linear blending method and the hyperbolic blending method was that the shape of the blending coefficients plots predicted by the hyperbolic blending method was smoother than that predicted by the linear blending method. In the following investigation, we will focus on the linear method.

As the drag force predicted by the linear blending method depends on the phase fraction and the diameters from both phases, it is necessary to compare the drag force predicted by the linear blending method and the traditional method as reported in Fig. 5 when a different value of the diameter of phase a is chosen. The

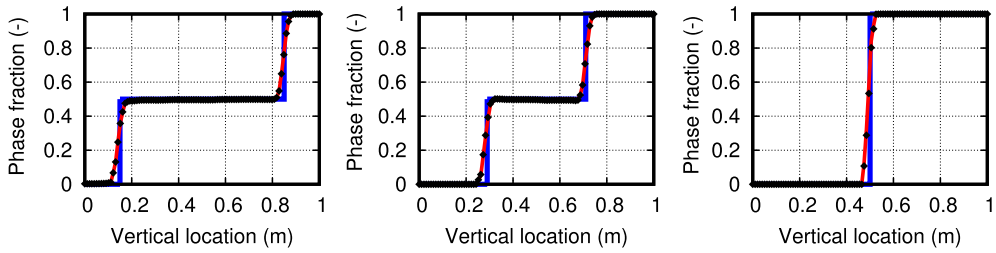

Fig. 2. Comparison of the air phase fraction distribution predicted by the fully conservative formulations (red line) and semi-conservative formulations (black points) with the analytical solution (blue line) at different time steps. (For interpretation of the references to colour in this figure legend, the reader is referred to the web version of this article.)

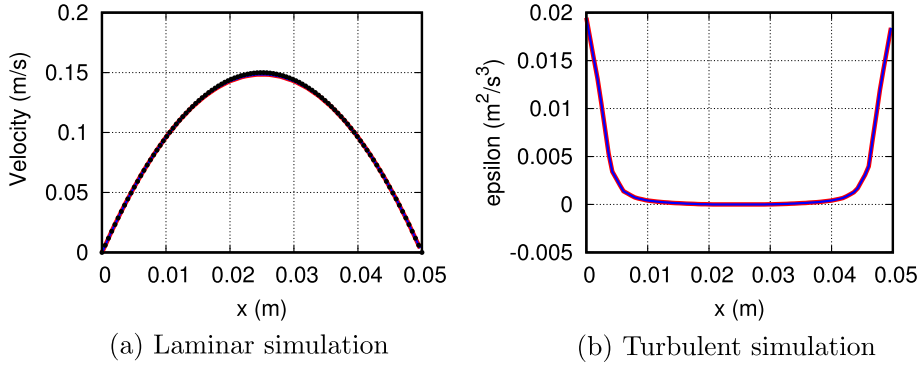

Fig. 3. (a): Comparison of the air velocity predicted by the semi-conservative (red line) and fully conservative (blue line) formulations with the analytical solution (black points). (b): Comparison of the turbulent energy dissipation rates of the air (red line) and water (blue line) predicted by the fully conservative formulation. (For interpretation of the references to colour in this figure legend, the reader is referred to the web version of this article.)

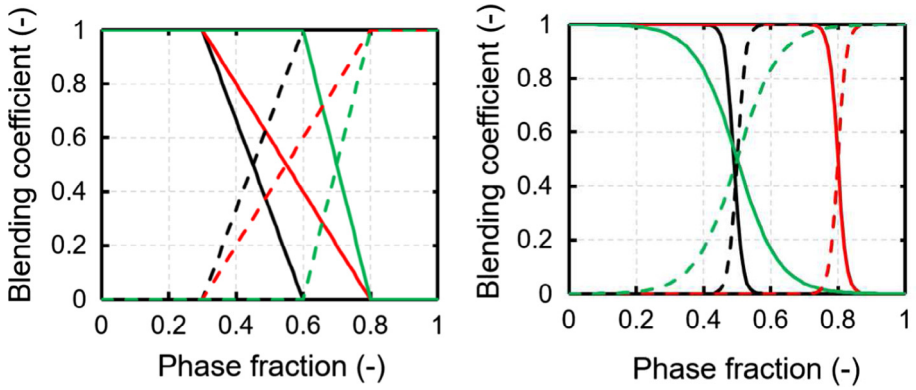

Fig. 4. Comparison of the blending coefficients f_a (solid lines) and f_b (dashed lines) predicted by the linear blending method (left) and the hyperbolic blending method (right). Black lines: $\alpha_{a,\mathrm{F}} = 0.3, \alpha_{a,\mathrm{P}} = 0.6, \alpha_{b,\mathrm{F}} = 0.4$, and $\alpha_{b,\mathrm{P}} = 0.7$ for the linear blending method; $\alpha_{a,\mathrm{F}} = 0.4, \alpha_{b,\mathrm{F}} = 0.6$, and $B_a = B_b = 0.1$ for the hyperbolic blending method. Red lines: $\alpha_{a,\mathrm{F}} = 0.3, \alpha_{a,\mathrm{P}} = 0.8, \alpha_{b,\mathrm{F}} = 0.2$, and $\alpha_{b,\mathrm{P}} = 0.7$ for the linear blending method; $\alpha_{a,\mathrm{F}} = 0.8, \alpha_{b,\mathrm{F}} = 0.8$, and $B_a = B_b = 0.1$ for the hyperbolic blending method. Blue lines: $\alpha_{a,\mathrm{F}} = 0.6, \alpha_{a,\mathrm{P}} = 0.8, \alpha_{b,\mathrm{F}} = 0.2$, and $\alpha_{b,\mathrm{P}} = 0.4$ for the linear blending method; $\alpha_{a,\mathrm{F}} = 0.5, \alpha_{b,\mathrm{F}} = 0.5$, and $B_a = B_b = 0.5$ for the hyperbolic blending method. (For interpretation of the references to colour in this figure legend, the reader is referred to the web version of this article.)

fluid parameters employed are reported in Table 1. The drag coefficient was calculated using the method from Schiller and Naumann (1935) owing to its simplicity. In Fig. 5(a), the phase fraction of a was set to 0.8, $f_a = 0.8$ and $f_b = 0.8$; in such cases, phase b can be seen as more dispersed than phase a and the contribution for the drag force mainly comes from phase b. It can be seen that the magnitude of the drag force predicted by the traditional method was much higher than that predicted by the linear blending method. Furthermore, the magnitude of the drag force predicted by the linear blending method was different when the diameter of phase b was employed, which was more physical. In Fig. 5(b), the phase fraction of a was set to 0.2, $f_a = 1$ and $f_b = 0$; in such cases, phase a was fully dispersed and the contribution for the drag force came from phase a. This was verified from the plot, which shows that the drag force predicted by the linear blending method overlapped with the plot of the drag force predicted using the old method. (see Table 2)

5.4. Three-dimensional bubble column simulations

In this section, the semi-conservative and fully conservative formulations, together with the two-phase $k-\varepsilon$ model, were employed to simulate a three-dimensional bubble column. The magnitude of the superficial velocity, $\mathbf{U}_G$, was given by 0.012 m/s, the time step was set to 0.002 s, and the linear blending method was employed. It should be stressed here that the CFL criterion

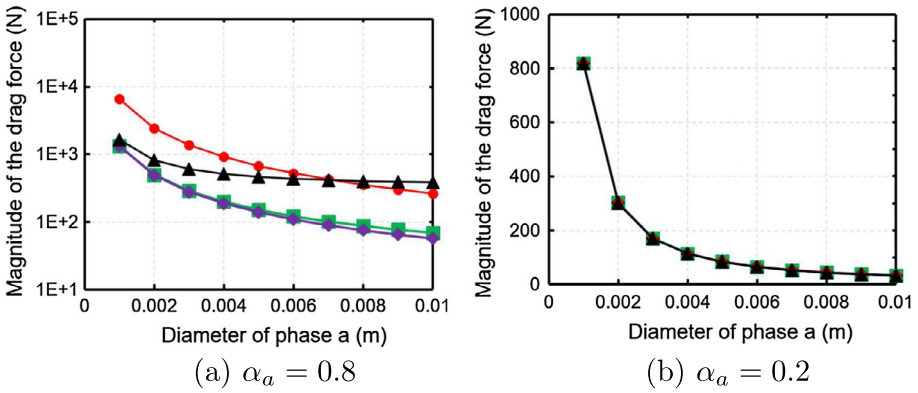

Fig. 5. Comparison of the drag forces predicted using the old method (red line) and the linear blending method (black line: $d_b = 1 \times 10^{-4}$ m; green line: $d_b = 5 \times 10^{-4}$ m; purple line: $d_b = 1 \times 10^{-3}$ m). (For interpretation of the references to colour in this figure legend, the reader is referred to the web version of this article.)

Table 1
Fluid parameters for the drag force predictions.

Relative velocity (m/s)	0.1
Density of phase *a* (kg/m^3)	1
Density of phase *b* (kg/m^3)	1000
Viscosity of phase *a* (Pas)	1×10^{-5}
Viscosity of phase *b* (Pas)	1×10^{-3}

Table 2
Comparison of the gas hold-up predicted by Díaz et al. and by this work with the experimental data.

Superficial velocity (m/s)	Experiments	Simulated in this work	Simulated by Díaz et al.
0.012	0.0263	0.0309	0.0221
0.0024	0.0069	0.0075	0.0064

should be satisfied to make the simulations converge; the time step effect on the flow fields will be discussed in the next section. As mentioned above, the issue for the semi-conservative and fully conservative formulations is the singularity, when the value of some phase fraction tends to be null. In the ANSYS CFX simulations by Díaz et al. (2008), the computational domain's height was equal to the liquid height. This is an effective way to prevent the phase segregation problem. In our simulations, the height of the computational domain was extended to be long enough to capture phase segregation and by this to verify the robustness of the semi-conservative and fully conservative formulations. The relative velocity predicted by the semi-conservative and fully conservative formulations, together with the time-averaged vertical liquid velocity and the time-averaged phase fraction predicted by the fully conservative formulation, is reported in Fig. 6, the plots of the instantaneous phase fraction, the continuous phase velocity vector and the disperse phase velocity vector are reported in Fig. 7. It can be seen that the value of the relative velocity above the liquid height predicted by both formulations tended to be null, which proves that, in such cases, the differential equations degenerate into algebraic equations and the velocity of each phase is assumed to be the same; otherwise, the singular problem arises. Furthermore, the contour plots of the time-averaged vertical liquid velocity and the time-averaged phase fraction predicted by the

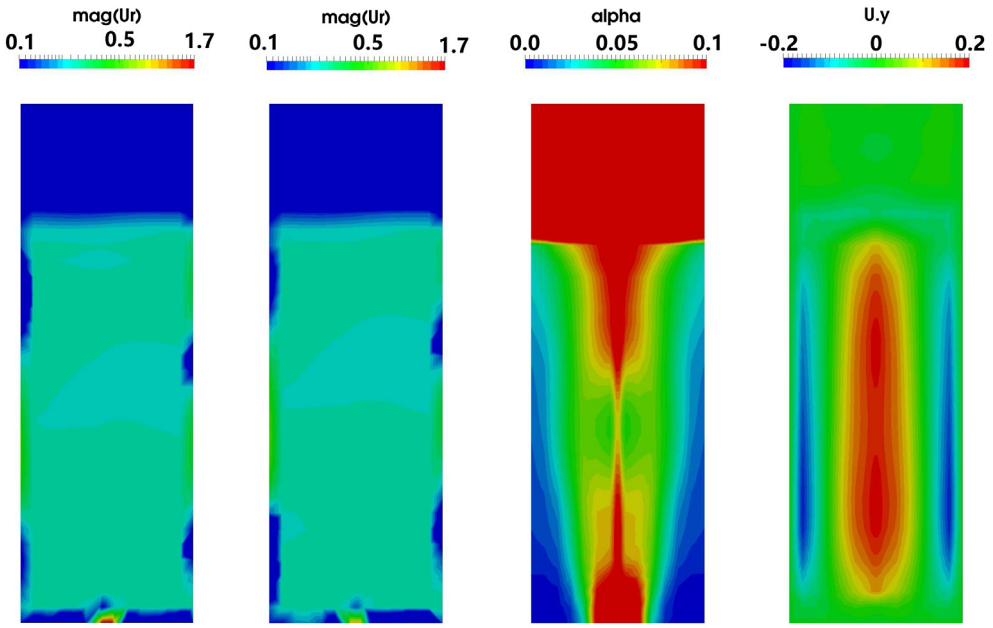

Fig. 6. Contour plots of the relative velocity predicted by the semi-conservative and fully conservative formulations, time-averaged dispersed phase fraction, and time-averaged magnitude of the vertical liquid velocity predicted by the semi-conservative formulations at mag($\mathbf{U}_G$) = 0.012 m/s (from left to right).

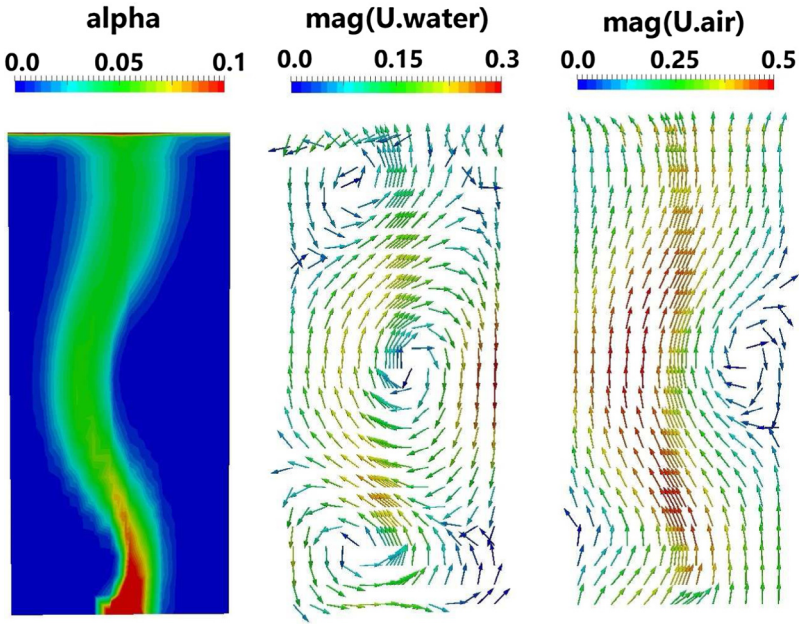

Fig. 7. Contour plots of the instantaneous phase fraction, continuous phase velocity vector and disperse phase velocity vector predicted by the fully conservative formulations at $\mathrm{mag}(\mathbf{U}_G) = 0.012$ m/s (from left to right).

fully conservative formulation were consistent with the simulation results by Díaz et al. (2008).

The comparison of the time-averaged phase fraction and the vertical liquid velocity at different bubble column heights predicted by the semi-conservative formulation and the fully conservative formulation with the results of Díaz et al. (2008) is reported in Fig. 8. It can be seen that the plot shape of the time-averaged phase fraction and the vertical liquid velocity agreed well with the results found by Díaz et al. (2008) and that the results predicted by the semi-conservative and fully conservative formulations overlapped. The predicted vertical liquid velocity, especially, presented an upward flow in the column center and a downward flow along the column walls, a phenomenon that is commonly referred to as the "gulf stream" or the "cooling tower" flow regime (Chen et al., 1989). The vortex flow is consistent with the plot of the continuous velocity vector as reported in Fig. 7.

The prediction of the time-averaged phase fraction in this work was slightly higher than the results in Díaz et al. (2008). Please note that we mostly compared to the previously reported numerical results by Díaz et al. (2008); the comparison of their numerical results to the experimental data can be found in their publication; the results for the gas hold-up are reported in Table 1. It can be seen that, when the superficial velocity was 0.012 m/s, the relative error of the gas hold-up predicted in this work was 17%, whereas that predicted by Díaz et al. (2008) was 16%. When the superficial velocity was 0.0024 m/s, the relative errors of the two were 8% and 7%, respectively. Both the relative errors increased when the superficial velocity increased. One reason for the remaining differences may be attributed to the assumption of a monodisperse distribution in this work, in which the bubble breakage and coalescence were not accounted for. They can play an important role in the highly turbulent gas-liquid dispersions under high superficial velocity conditions. Better results might be obtained by simulations with a CFD coupled with a population balance model, which could be interesting for future studies.

5.5. Choice of the time step

It is also interesting to investigate the time step effect on the flow fields as the horizontal liquid velocity behaves very periodically. Usually, the bubble plumes show a wavelike motion, which is an essential characteristic of partially aerated bubble columns. In this section, the magnitude of $\mathbf{U}_G$ was given by 0.0024 m/s and the linear blending method was employed. The CFL condition is reported by

$$\Delta t < \frac{\Delta y}{|\mathbf{U}|}, \tag{48}$$

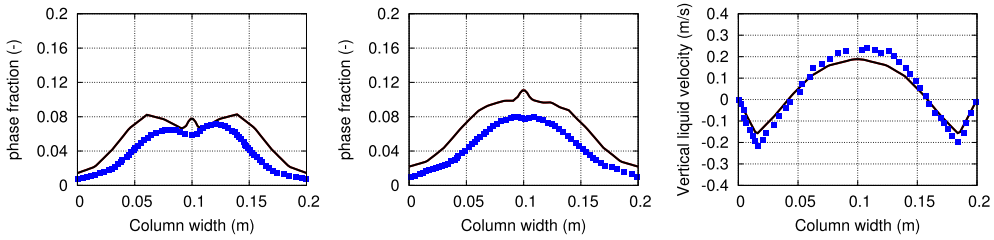

(a) $H = 0.2$ m (b) $H = 0.3$ m (c) $H = 0.2$ m

Fig. 8. Comparison of the time-averaged phase fraction and vertical liquid velocity at different bubble column heights predicted by the semi-conservative formulation (red line) and the fully conservative formulation (black line) with the results of Díaz et al. (2008) (blue squares) at $\mathrm{mag}(\mathbf{U}_G) = 0.012$ m/s. Simulations were run for 300 s, and the time averaging started at 150 s. (For interpretation of the references to colour in this figure legend, the reader is referred to the web version of this article.)

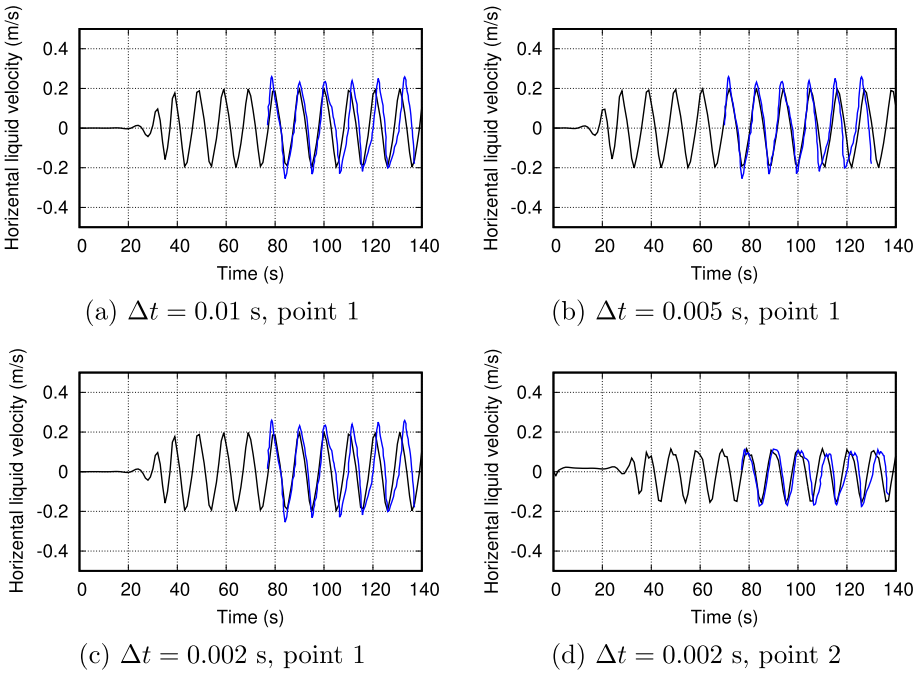

Fig. 9. Comparison between the prediction of the horizontal liquid velocity from the fully conservative formulations (black lines) and the results found by Díaz et al. (2008) (blue lines) with different time steps at different points. Point 1: $x = 0.1$ m, $y = 0.225$ m, $z = 0.02$ m. Point 2: $x = 0.05$ m, $y = 0.225$ m, $z = 0.02$ m. (For interpretation of the references to colour in this figure legend, the reader is referred to the web version of this article.)

where Δy is the characteristic dimension of the cell and Δt is the time step. For this test case, three different time steps were chosen, namely, $\Delta t = 0.002$ s, $\Delta t = 0.005$ s, and $\Delta t = 0.01$ s. The maximum Courant number for these time steps was 0.14, 0.32, and 0.65, respectively. The predicted horizontal liquid velocities at different points are reported in Fig. 9. It can be seen that all the horizontal liquid velocities predicted by these time steps behaved periodically after enough relaxation time (e.g., 50 s). Not only the period but also the peak horizontal liquid velocity predicted by the fully conservative formulations with the two-phase $k-\varepsilon$ model also agreed well with the data provided by Díaz et al. (2008). As mentioned before, the magnitude of the horizontal liquid velocity is sensitive to the turbulent response coefficient, which can only be predicted accurately by the two-phase $k-\varepsilon$ model. The predicted instantaneous phase fraction, air velocity, and water velocity were compared with the data provided in Díaz et al. (2008), as reported in Fig. 7. It can be seen that the experimental and simulated results were in good agreement.

5.6. Prediction of the drag force

It can be seen from Eq. (42) that the drag force predicted by the blending method was dependent on the parameters (e.g., diameter for phase a and phase b) of both phases. However, the predicted drag force should be independent of the diameter of the continuous phase. In this section, the effect of the diameter of the continuous phase on the predicted drag force using the linear blending method and the traditional method was investigated.

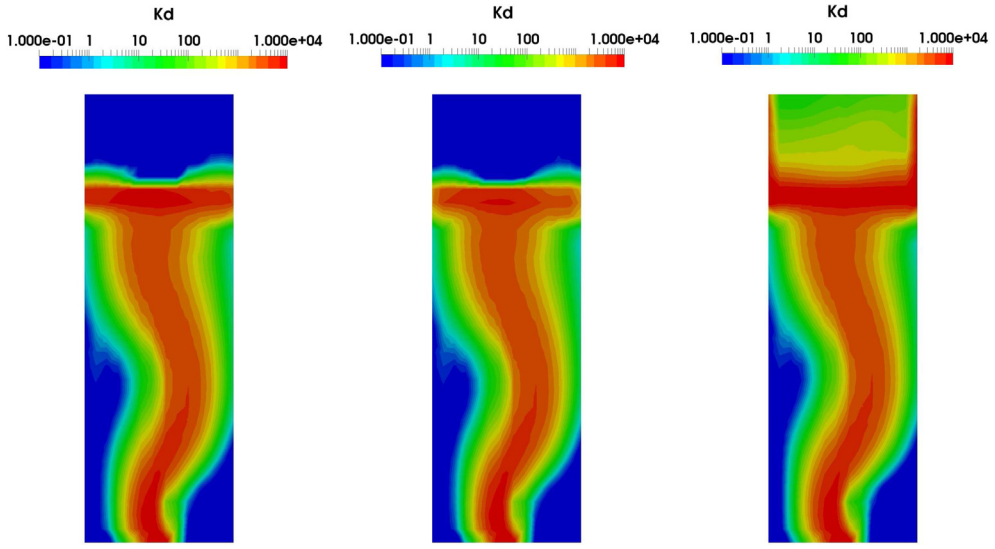

Fig. 10. Contour plots of Kd predicted by the linear blending method when $d_c = 1 \times 10^{-5}$ m (left) and $d_c = 5 \times 10^{-5}$ m (middle) and by the traditional method (right).

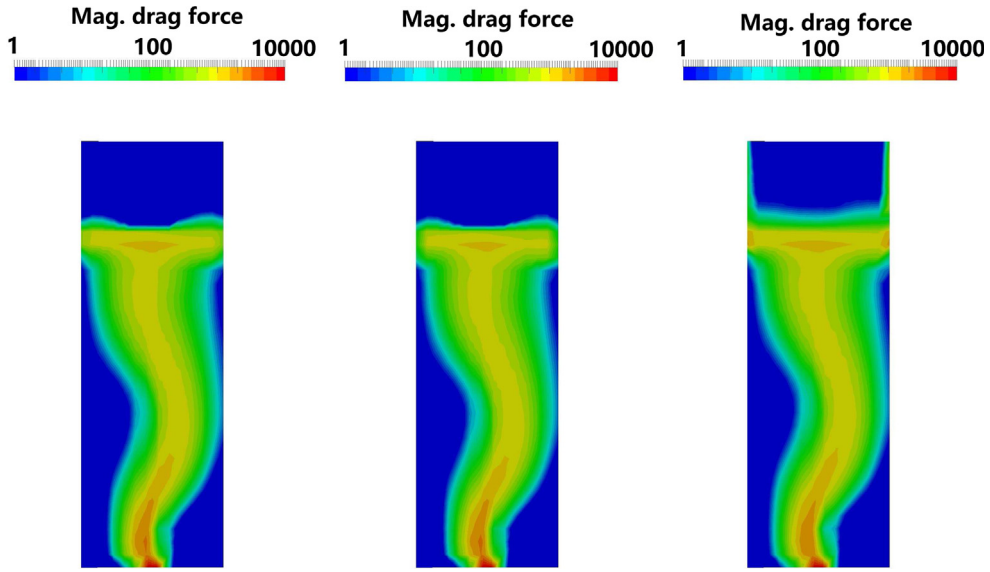

Fig. 11. Contour plots of the magnitude of the drag force predicted by the linear blending method when $d_c = 1 \times 10^{-5}$ m (left) and $d_c = 5 \times 10^{-5}$ m (middle) and by the traditional method (right).

The parameters for the linear blending method are given by $\alpha_{a,\mathrm{F}} = 0.6, \alpha_{a,\mathrm{P}} = 0.9, \alpha_{b,\mathrm{F}} = 0.1$, and $\alpha_{b,\mathrm{F}} = 0.4$. It can be seen in Fig. 10 that the value of Kd in Eq. (18) or Eq. (19) predicted by the linear blending method using different diameters of water is similar. This proves that the predicted value of Kd is independent of the given diameter of the water. Furthermore, the predicted value of Kd was very small above the water surface, which is consistent with the physics as water becomes dispersed in such regions. For the traditional method, the predicted value of Kd was consistent with the predictions from the linear blending method in those regions below the water surface. However, the predicted value of Kd was not correct in the regions above the water surface as, even in such regions, Kd is still calculated from the parameters of the air, which does not obey the physics as the air phase is not dispersed. This non-physical prediction of Kd may introduce unstable calculations. It is also interesting to compare the drag force predicted by the linear blending method and the traditional method, as reported in Fig. 11. Similarly to the prediction of Kd, the drag force predicted by the linear blending method was similar when different diameters of water were given. It can also be seen that the drag force predicted by the traditional method was acceptable. This is because, in the region above the water surface, the phase fraction of water is lower than α_s and, thus, a phase segregation occurs; the differential phase momentum equations degenerate into algebraic phase momentum equations, which means that $|\mathbf{U}_\mathrm{r}| \approx 0$, namely, $\mathbf{M}_\mathrm{drag} \approx 0$.

6. Conclusions

The two-fluid model (TFM) is widely used to simulate gas-liquid bubble columns. One of the difficulties when solving the governing equations numerically is how to prevent the "singular" problem in the case of phase segregation. A similar problem also occurs when a fully conservative two-phase turbulent model is applied. This work analyzed the semi-conservative and fully conservative TFM equations, together with the fully conservative two-phase $k-\varepsilon$ model with the bubble-induced turbulence source terms implemented in OpenFOAM. Special numerical treatments were applied for the drag force to prevent the singular problem in the phase momentum equations. Similar numerical treatments were also applied for the source term in the two-phase $k-\varepsilon$ model. In addition, two new methods were proposed to calculate the drag force, namely, the linear blending method and the hyperbolic blending method, and their capabilities were also investigated. Finally, the flow fields predicted by the semi-conservative and fully conservative formulations, together with the two-phase $k-\varepsilon$ model, the linear blending method, and the hyperbolic blending method, were compared with experimental data, providing our simulations with the necessary validation.

Our zero-dimensional results showed that, by using the special numerical treatment on the drag force, the singular problem can be prevented for both the semi-conservative and the fully conservative formulations. Our three-dimensional bubble column simulation results proved that the flow fields predicted by both the semi-conservative and the fully conservative formulation agreed well with the literature data. The TFM, combined with the two-phase $k-\varepsilon$ model, produced satisfactory predictions of the horizontal liquid velocity, yielding good predictions of the plume oscillation. The drag forces predicted by the linear blending method and the hyperbolic blending method were more reasonable than the predictions using the traditional method. Last but not least, the drag force predicted by the blending method was not dependent on the diameter of the continuous phase if adequate blending coefficients were chosen, and the blending method was more suitable than the traditional method when there was phase inversion.

References

Alopaeus, V., Koskinen, J., Keskinen, K., Majander, J., 2002. Simulation of the population balances for liquid–liquid systems in a non-ideal stirred tank. Part 2–Parameter fitting and the use of the multiblock model for dense dispersions. Chem. Eng. Sci. 57, 1815–1825.

Antal, S., Lahey, R., Flaherty, J., 1991. Analysis of phase distribution in fully developed laminar bubbly two-phase flow. Int. J. Multiphase Flow 17, 635–652.

Arnold, G., Drew, D., Lahey, J., 1989. Derivation of constitutive equations for interfacial force and Reynolds stress for a suspension of spheres using ensemble cell averaging. Chem. Eng. Commun. 86, 43–54. T., R.,.

Bajorek, S., 2008. TRACE V5.0 theory manual, field equations, solution methods and physical models. United States Nuclear Regulatory Commission.

Becker, S., De Bie, H., Sweeney, J., 1999. Dynamic flow behaviour in bubble columns. Chem. Eng. Sci. 54, 4929–4935.

Behzadi, A., Issa, R., Rusche, H., 2004. Modelling of dispersed bubble and droplet flow at high phase fractions. Chem. Eng. Sci. 59, 759–770.

Besbes, S., El Hajem, M., Ben Aissia, H., Champagne, J., Jay, J., 2015. PIV measurements and Eulerian–Lagrangian simulations of the unsteady gas–

liquid flow in a needle sparger rectangular bubble column. Chem. Eng. Sci. 126, 560–572.
Bhusare, V., Dhiman, M., Kalaga, D., Roy, S., Joshi, J., 2017. CFD simulations of a bubble column with and without internals by using OpenFOAM. Chem. Eng. J. 317, 157–174.
Brilliantov, N., Spahn, F., Hertzsch, J., Pöschel, T., 1996. Model for collisions in granular gases. Phys. Rev. E 53, 5382.
Buffo, A., De Bona, J., Vanni, M., Marchisio, D., 2016. Simplified volume-averaged models for liquid–liquid dispersions: correct derivation and comparison with other approaches. Chem. Eng. Sci. 153, 382–393.
Buffo, A., Marchisio, D., Vanni, M., Renze, P., 2013a. Simulation of polydisperse multiphase systems using population balances and example application to bubbly flows. Chem. Eng. Res. Des. 91, 1859–1875.
Buffo, A., Vanni, M., Marchisio, D., Fox, R., 2013b. Multivariate quadrature-based moments methods for turbulent polydisperse gas–liquid systems. Int. J. Multiphase Flow 50, 41–57.
Buwa, V., Deo, D., Ranade, V., 2006. Eulerian–Lagrangian simulations of unsteady gas–liquid flows in bubble columns. Int. J. Multiphase Flow 32, 864–885.
Cano-Pleite, E., Hernández-Jiménez, F., Acosta-Iborra, A., 2015. Compressible-gas two-fluid modeling of isolated bubbles in a vertically vibrated fluidized bed and comparison with experiments. Chem. Eng. J. 271, 287–299.
Chen, J., Jamialahmadi, M., Li, S., 1989. Effect of liquid depth on circulation in bubble columns: a visual study. Chem. Eng. Res. Des. 67, 203–207.
Cundall, P., Strack, O., 1979. A discrete numerical model for granular assemblies. Geotechnique 29, 47–65.
De Bona, J., Buffo, A., Vanni, M., Marchisio, D., 2016. Limitations of simple mass transfer models in polydisperse liquid–liquid dispersions. Chem. Eng. J. 296, 112–121.
Deckwer, W., Field, R., 1992. Bubble Column Reactors, vol. 200. Wiley, New York.
Díaz, M., Iranzo, A., Cuadra, D., Barbero, R., Montes, F., Galán, M., 2008. Numerical simulation of the gas–liquid flow in a laboratory scale bubble column: influence of bubble size distribution and non-drag forces. Chem. Eng. J. 139, 363–379.
Dopazo, C., 1977. On conditioned averages for intermittent turbulent flows. J. Fluid Mech. 81, 433–438.
Drew, D., 1982. Mathematical modeling of two–phase flow. Annu. Rev. Fluid Mech. 15, 261–291.
Drew, D., Passman, S., 2006. Theory of Multicomponent Fluids, vol. 135. Springer.
El Tahry, S., 1983. k-epsilon equation for compressible reciprocating engine flows. J. Energy 7, 345–353.
Gao, Z., Li, D., Buffo, A., Podgórska, W., Marchisio, D., 2016. Simulation of droplet breakage in turbulent liquid–liquid dispersions with CFD-PBM: Comparison of breakage kernels. Chem. Eng. Sci. 142, 277–288.
Gosman, A., Lekakou, C., Politis, S., Issa, R., Looney, M., 1992. Multidimensional modeling of turbulent two–phase flows in stirred vessels. AIChE J. 38, 1946–1956.
Grace, J., Wairegi, T., Nguyen, T., 1976. Shapes and velocities of single drops and bubbles moving freely through immiscible liquids. Chem. Eng. Res. Des. 54, 167–173.
Hanjalic, K., Launder, B., 1972. A Reynolds stress model of turbulence and its application to thin shear flows. J. Fluid Mech. 52, 609–638.
Hibiki, T., Ishii, M., 2003. One-dimensional drift-flux model and constitutive equations for relative motion between phases in various two-phase flow regimes. Int. J. Heat Mass Transfer 46, 4935–4948.
Hill, D., 1998. The computer simulation of dispersed two-phase flow. Ph.D. thesis, University of London.
Hjertager, B., 1998. Computational fluid dynamics (CFD) analysis of multiphase chemical reactor. Trends Chem. Eng.
Höhne, T., Mehlhoop, J., 2014. Validation of closure models for interfacial drag and turbulence in numerical simulations of horizontal stratified gas–liquid flows. Int. J. Multiphase Flow 62, 1–16.
Hoomans, B., Kuipers, J., Briels, W., Van-Swaaij, W., 1996. Discrete particle simulation of bubble and slug formation in a two-dimensional gas-fluidised bed: a hard-sphere approach. Chem. Eng. Sci. 51, 99–118.
Ishii, M., 1975. Thermo-fluid dynamic theory of two-phase flow. NASA STI/Recon Tech. Rep. A 75, 29657.
Ishii, M., 1977. One-dimensional drift-flux model and constitutive equations for relative motion between phases in various two-phase flow regimes. Argonne National Laboratory Report, ANL-77-47.
Ishii, M., Hibiki, T., 2010. Thermofluid Dynamics of Two-phase Flow. Springer Science & Business Media.
Ishii, M., Mishima, K., 1984. Two-fluid model and hydrodynamic constitutive relations. Nucl. Eng. Des. 82, 107–126.
Ishii, M., Zuber, N., 1979. Drag coefficient and relative velocity in bubbly, droplet or particulate flows. AIChE J. 25, 843–855.
Issa, R., Gosman, A., Watkins, A., 1986. The computation of compressible and incompressible recirculating flows by a non-iterative implicit scheme. J. Comput. Phys. 62, 66–82.
Jain, D., Kuipers, J., Deen, N., 2014. Numerical study of coalescence and breakup in a bubble column using a hybrid volume of fluid and discrete bubble model approach. Chem. Eng. Sci. 119, 134–146.
Jakobsen, H., Sannæs, B., Grevskott, S., Svendsen, H., 1997. Modeling of vertical bubble-driven flows. Indust. Eng. Chem. Res. 36, 4052–4074.
Jeong, J., Ha, K., Chung, B., Lee, W., 1999. Development of a multi-dimensional thermal-hydraulic system code, MARS 1.3.1. Ann. Nucl. Energy 26, 1611–1642.
Kantarci, N., Borak, F., Ulgen, K., 2005. Bubble column reactors. Process Biochem. 40, 2263–2283.
Karema, H., Lo, S., 1999. Efficiency of interphase coupling algorithms in fluidized bed conditions. Comput. Fluids 28, 323–360.
Lahey, R., 1990. The analysis of phase separation and phase distribution phenomena using two-fluid models. Nucl. Eng. Des. 122, 17–40.
Lahey, R., 2005. The simulation of multidimensional multiphase flows. Nucl. Eng. Des. 235, 1043–1060.
Lamb, H., 1932. Hydrodynamics. Cambridge University Press.
Lau, Y., Sujatha, K., Gaeini, M., Deen, N., Kuipers, J., 2013. Experimental study of the bubble size distribution in a pseudo-2d bubble column. Chem. Eng. Sci. 98, 203–211.
Launder, B., Spalding, D., 1974. The numerical computation of turbulent flows. Comput. Methods Appl. Mech. Eng. 3, 269–289.
Li, D., Buffo, A., Podgórska, W., Gao, Z., Marchisio, D., 2017. Droplet breakage and coalescence in liquid-liquid dispersions: comparison of different kernels with EQMOM and QMOM. AIChE J. 63, 2293–2311.
Li, D., Buffo, A., Podgórska, W., Marchisio, D., Gao, Z., in press. Investigation of droplet breakup in liquid-liquid dispersions by CFD-PBM simulations: the influence of the surfactant type. Chinese J. Chem. Eng, in press.
Liu, Y., Hinrichsen, O., 2014. Study on CFD–PBM turbulence closures based on $k-\varepsilon$ and Reynolds stress models for heterogeneous bubble column flows. Comput. Fluids 105, 91–100.
Lopez De Bertodano, M., 1992. Turbulent bubbly two-phase flow in a triangular duct. Ph.D. thesis, Rensselaer Polytechnic Institute.
Lopez De Bertodano, M., Fullmer, W., Clausse, A., Ransom, V., 2016. Two-Fluid Model Stability, Simulation and Chaos. Springer.
Lopez De Bertodano, M., Lahey, R., Jones, O., 1994. Development of a $k-\varepsilon$ model for bubbly two-phase flow. J. Fluids Eng. 116, 128–134.
Lopez De Bertodano, M., Lee, S., Lahey, R., Drew, D., 1990. The prediction of two-phase turbulence and phase distribution phenomena using a Reynolds stress model. J. Fluids Eng. 112, 107–113.
Maaß, S., Metz, F., Rehm, T., Kraume, M., 2010. Prediction of drop sizes for liquid–liquid systems in stirred slim reactors–Part I: Single stage impellers. Chem. Eng. J. 162, 792–801.
Miller, T., Miller, D., 2003. A fourier analysis of the IPSA/PEA algorithms applied to multiphase flows with mass transfer. Comput. Fluids 32, 197–221.
Muzaferija, S., Perić, M., 1997. Computation of free-surface flows using the finite-volume method and moving grids. Numer. Heat Transfer 32, 369–384.
Oliveira, P., Issa, R., 1994. On the numerical treatment of interphase forces in two-phase flow. ASME Publications Fed. 185. 131-131.
Oliveira, P., Issa, R., 2003. Numerical aspects of an algorithm for the Eulerian simulation of two-phase flows. Int. J. Numer. Methods Fluids 43, 1177–1198.
Park, I., Cho, H., Yoon, H., Jeong, J., 2009. Numerical effects of the semi-conservative form of momentum equations for multi-dimensional two-phase flows. Nucl. Eng. Des. 239, 2365–2371.
Park, J., Drew, D., Lahey, R., 1999. The analysis of void wave propagation in adiabatic monodispersed bubbly two-phase flows using an ensemble-averaged two-fluid model. Int. J. Multiphase Flow 24, 1205–1244.
Passalacqua, A., Fox, R., 2011. Implementation of an iterative solution procedure for multi-fluid gas–particle flow models on unstructured grids. Powder Technol. 213, 174–187.
Petitti, M., Nasuti, A., Marchisio, D., Vanni, M., Baldi, G., Mancini, N., Podenzani, F., 2010. Bubble size distribution modeling in stirred gas–liquid reactors with QMOM augmented by a new correction algorithm. AIChE J. 56, 36–53.
Petitti, M., Vanni, M., Marchisio, D., Buffo, A., Podenzani, F., 2013. Simulation of coalescence, break-up and mass transfer in a gas–liquid stirred tank with CQMOM. Chem. Eng. J. 228, 1182–1194.
Rhie, C., Chow, W., 1983. Numerical study of the turbulent flow past an airfoil with trailing edge separation. AIAA J. 21, 1525–1532.
Roghair, I., Lau, Y., Deen, N., Slagter, H., Baltussen, M., Annaland, M., Kuipers, J., 2011. On the drag force of bubbles in bubble swarms at intermediate and high Reynolds numbers. Chem. Eng. Sci. 66, 3204–3211.
Rusche, H., 2003. Computational fluid dynamics of dispersed two–phase flows at high phase fractions. Ph.D. thesis, Imperial College London.
Saurel, R., Abgrall, R., 1999. A multiphase Godunov method for compressible multifluid and multiphase flows. J. Comput. Phys. 150, 425–467.
Schiller, L., Naumann, A., 1935. A drag coefficient correlation. VDI Zeitung 77, 51–86.
Shaikh, A., Al-Dahhan, M., 2007. A review on flow regime transition in bubble columns. Int. J. Chem. Reactor Eng. 5, 560–572.
Sharma, S., Hibiki, T., Ishii, M., Schlegel, J., Buchanan, J., Hogan, K., Guilbert, P., 2017. An interfacial shear term evaluation study for adiabatic dispersed air–water two-phase flow with the two-fluid model using CFD. Nucl. Eng. Des. 312, 389–398.
Singh, B., Quiyoom, A., Buwa, V., 2017. Dynamics of gas–liquid flow in a cylindrical bubble column: comparison of electrical resistance tomography and voidage probe measurements. Chem. Eng. Sci. 158, 124–139.
Sokolichin, A., Eigenberger, G., Lapin, A., Lübert, A., 1997. Dynamic numerical simulation of gas-liquid two-phase flows Euler/Euler versus Euler/Lagrange. Chem. Eng. Sci. 52, 611–626.
Spalding, D., 1980. Numerical computation of multi-phase fluid flow and heat transfer. Recent Adv. Numer. Methods Fluids 1, 139–167.
Stadtke, H., 2006. Gasdynamic Aspects of Two-phase Flow. Wiley-Vch.
Tomiyama, A., Tamai, H., Zun, I., Hosokawa, S., 2002. Transverse migration of single bubbles in simple shear flows. Chem. Eng. Sci. 57, 1849–1858.

Vaidheeswaran, A., Lopez De Bertodano, M., 2017. Stability and convergence of computational Eulerian two-fluid model for a bubble plume. Chem. Eng. Sci. 160, 210–226.
Wang, S., Luo, K., Yang, S., Hu, C., Fan, J., 2017. Parallel LES-DEM simulation of dense flows in fluidized beds. Appl. Therm. Eng. 111, 1523–1535.
Weller, H., 2002. Derivation, modelling and solution of the conditionally averaged two-phase flow equations. Nabla Ltd, Technical Report TR/HGW/02.
Yoshida, H., Ohnuki, A., Misawa, T., Takase, K., Akimoto, H., 2008. Development of analytical procedures of two-phase flow in tight-lattice fuel bundles for innovative water reactor for flexible fuel cycle. Nucl. Technol. 164, 45–54.
Zhang, D., Deen, N., Kuipers, J., 2006. Numerical simulation of the dynamic flow behavior in a bubble column: a study of closures for turbulence and interface forces. Chem. Eng. Sci. 61, 7593–7608.
Zhang, S., Zhao, X., Bayyuk, S., 2014. Generalized formulations for the Rhie-Chow interpolation. J. Comput. Phys. 258, 880–914.
Zhu, H., Zhou, Z., Yang, R., Yu, A., 2007. Discrete particle simulation of particulate systems: theoretical developments. Chem. Eng. Sci. 62, 3378–3396.